PASJ: Publ. Astron. Soc. Japan **61**, 461–469, 2009 June 25

A Large Expanding Molecular Arc in the Sagittarius B1 Complex

Kunihiko TANAKA
Nobeyama Radio Observatory, 462-2 Minamimaki, Minamisaku, Nagano 384-1805
ktanaka@nro.nao.ac.jp
Tomoharu OKA
Institute of Science and Technology, Keio University, 4-14-1 Hiyoshi, Yokohama, Kanagawa 223-8522
Makoto NAGAI
Institute of Physics, University of Tsukuba, 1-1-1 Ten-nodai, Tsukuba, Ibaraki 305-8577
and
Kazuhisa KAMEGAI
Institute of Space and Astronautical Science, Japan Aerospace Exploration Agency, 3-1-1 Yoshinodani, Sagamihara, Kanagawa 229-8510

(Received 2008 June 17; accepted 2009 January 4)

Abstract

Results of molecular line observations toward the Sagittarius B1 complex are reported. Maps of the HCN, HCO^+ and SiO $J = 1$–0 emissions were taken with the NRO 45-m telescope. With these data, combined with the ASTE CO $J = 3$–2 survey data, we have investigated the spatial structure, kinematics and physical conditions of two peculiar molecular features: CO0.55+0.07 and SiO0.56−0.01. The CO arc, CO0.55+0.07, shows clear expanding motion with sizes of $8.5 \times 6.8\,\mathrm{pc}^2$ and an expansion velocity of $40\,\mathrm{km\,s^{-1}}$. The SiO shell, SiO0.56−0.01, has a size of $3.0 \times 3.4\,\mathrm{pc}^2$, and surrounds an X-ray Fe line source, G0.570−0.018. The mass and the kinetic energy of CO0.55+0.07 are estimated to be $10^{5.5}\,M_\odot$ and $10^{51.5}$ erg, respectively. The kinetic energy of SiO0.56−0.01 is $\sim 10^{50.4}$ erg. An LVG analysis shows that the typical density and kinetic temperature are $10^{3.8}\,\mathrm{cm^{-3}}$ and 28 K, respectively. High-density clumps with a density of $10^{4.0-4.5}\,\mathrm{cm^{-3}}$ associated with CO0.55+0.07 and SiO0.56−0.01 have been found, supporting the idea that they consist of swept-up material. The huge kinetic energy of CO0.55+0.07 is considered to be injected by a series of supernova explosions that took place within $\sim 2 \times 10^5$ yr, which would suggest that it is a 'bubble' created by a massive stellar cluster, whose mass is estimated to be $10^{3.5-4.5}\,M_\odot$. The origin of SiO0.56−0.01 is rather unclear, but we suggest that it could be related to the X-ray source G0.570−0.018.

Key words: Galaxy: center — ISM: bubbles — ISM: clouds

1. Introduction

The inner 200 pc of our Galaxy is called the Central Molecular Zone (CMZ), containing a large concentration of dense molecular gas. The molecular clouds there have an anomalous physical condition characterized by high density, $\sim 10^4\,\mathrm{cm^{-3}}$, high gas kinetic temperature, 30–60 K, and large velocity dispersion, $\gtrsim 40\,\mathrm{km\,s^{-1}}$ (Morris et al. 1983; Oka et al. 1998; Martin et al. 2004; Nagai et al. 2007). Surveys of molecular lines and dust continuum in the millimeter and submillimeter wavelengths (Oka et al. 1998; Tsuboi et al. 1999; Pierce-Price et al. 2000) revealed the complicated structure of the CMZ, which contains a number of filaments, arcs and shells, indicating the presence of pervasive shock, which is also suggested by the peculiar chemical composition of the molecular gas (Martín-Pintado et al. 1997; Hüttemeister et al. 1998; Requena-Torres et al. 2008). For the origin of the shock, several explanations are proposed, including cloud-cloud collision caused by orbit crowding (Hüttemeister et al. 1998) and magnetic floatation (Fukui et al. 2006).

Recent molecular line observations found peculiar molecular clouds with expanding motion of extraordinarily high energy, possibly caused by interactions with local energetic phenomena. A CO $J = 3$–2 survey with the ASTE 10-m telescope (Oka et al. 2007) found a number of 'hot spots' with a high CO $(J = 3\text{–}2)/(J = 1\text{–}0)$ intensity ratio, many of which are classified as high-velocity compact clouds (HVCCs), having a large velocity width ($\gtrsim 50\,\mathrm{km\,s^{-1}}$) and enormous kinetic energy ($\sim 10^{50-52}$ erg). Tanaka et al. (2007) found multiple expanding shells with a kinetic energy of 10^{50-52} erg in the $l = 1.^\circ3$ complex, suggesting that it could be a 'proto-superbubble' formed by supernova (SN) explosions of massive stellar clusters comparable to those in the Sgr A and the Radio Arc regions (Figer et al. 1999, 2002; Paumard et al. 2006). These results may imply that the molecular clouds in the CMZ are perturbed by SN explosions, though the energetic shells, arcs and HVCCs are rarely associated with known radio/X-ray SNRs or stellar clusters.

The molecular arc CO0.55+0.07 is a unique molecular feature, since it is located in the Sagittarius B complex, the most active star-forming region in the CMZ. The cloud, which has a typical kinematics of an expanding arc, was first recognized by a CO $J = 1$–0 survey (Oka et al. 1998). The Sgr B complex is known for burst-like star formation (Mehringer et al. 1992, 1993), and contains a number of H II regions and X-ray Fe line sources (Koyama et al. 2007); it is strongly suggested that the arc is formed via interactions with energetic sources related to the star-formation activity.

Table 1. Observed lines.

Transition	Frequency (GHz)	Beam (″)	Grid (″)	$1/\eta_{\rm MB}$
HCN $J = 1$–0	88.63	19	20.55	2.5
HCO^+ $J = 1$–0	88.69751	19	20.55	2.5
SiO $J = 1$–0	43.42376	38	41.1, 82.2	1.3
CO* $J = 3$–2	345.79599	22	34	

* Taken from Oka et al. (2007).

This paper reports on the results of molecular line mappings of the Sgr B1 complex, which we performed to detect shocked gas associated with CO0.55+0.07. With these data and the CO $J = 3$–2 data taken with the ASTE survey, we estimate the kinetic energy of the arc and discuss the possibility that the arc is created through interactions with SN explosions similarly to the proto-superbubble in the $l = 1.^\circ3$ complex. We also report on the discovery of an SiO shell that could be associated with a peculiar X-ray iron line source.

2. Observations

The observations were carried out by using the Nobeyama Radio Observatory (NRO) 45-m telescope in 2007 April. The observed lines were HCN, HCO^+, and thermal SiO $J = 1$–0 emissions. The observed frequencies and respective angular resolutions are listed in table 1. For observations of the HCN and HCO^+ lines, the BEARS 25 multi-beam receiver system was used. The digital backend was operated in the wide-band mode with 0.5 MHz channel widths. The SiO $J = 1$–0 line was observed with the S40 receiver, and the AOS-H with a 250 kHz channel width.

The spectra were smoothed by a 2 km s^{-1} FWHM Gaussian, and regridded onto each 2 km s^{-1} bin. Antenna temperatures were calibrated by a chopper-wheel method. The correction factor for the main-beam efficiency ($1/\eta_{\rm MB}$) adopted for each line is listed in table 1. The antenna pointing accuracy was maintained within 3″ during the observation run by observing the SiO $J = 1$–0, $v = 1,2$ maser lines toward VX-Sgr. All of the observations were carried out in a position-switching mode. The reference position was taken at $(l, b) = (1^\circ, -1^\circ)$.

The mapped region covered 7′ × 7′ area centered at $(l, b) = (0.^\circ57, 0^\circ)$. The grid separation was 20.″55 for the HCN and HCO^+ observations. The SiO spectra was taken at 82.″2 grid separation for the 7′ × 7′ region, and at 41.″1 separation for the central 5′ × 5′ region.

We also used the CO $J = 3$–2 data taken with the ASTE 10-m telescope. The details of the ASTE observation are described in Oka et al. (2007).

3. Results

3.1. CO0.55+0.07: Large Expanding Arc

Figure 1 shows the distribution of the CO $J = 3$–2, HCN and HCO^+ intensity at the $v_{\rm LSR} = 50$, 60, and 70 km s^{-1} velocity channels. The molecular arc CO0.55+0.07 is seen as a semi-elliptical emission cavity centered at $(l, b) = (0.^\circ56, 0.^\circ07)$ in each map. Its expanding motion is most clearly seen in the l–v diagram at $b = 0.^\circ07$, presented in figure 2. The region with intense emission has a 'U'-shaped morphology in the l–$v_{\rm LSR}$ diagrams, which is characteristic of an expanding cloud.

We assumed that the spatial structure and the kinematics of CO0.55+0.07 can be represented by a proportionally expanding ellipsoid, whose axes are parallel to the l, b and

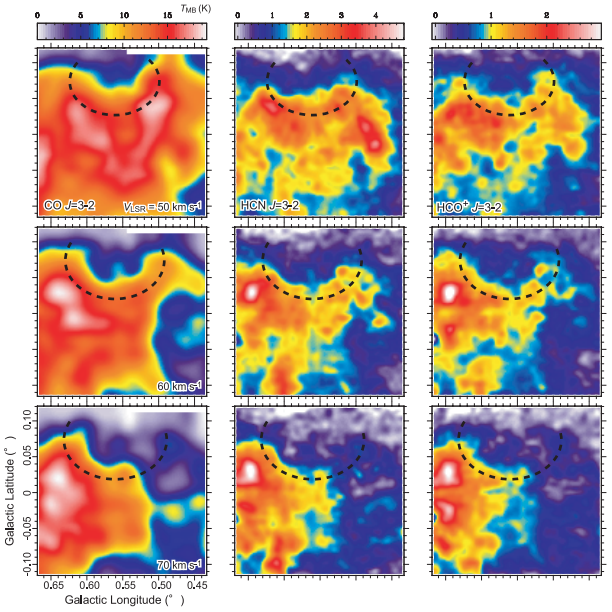

Fig. 1. Intensity of the CO $J = 3$–2, HCN $J = 1$–0 and HCO^+ $J = 1$–0 emissions at $v_{\rm LSR} = 50$, 60, and 70 km s^{-1}. The dashed lines represent the model of the expanding motion defined by equation (1).

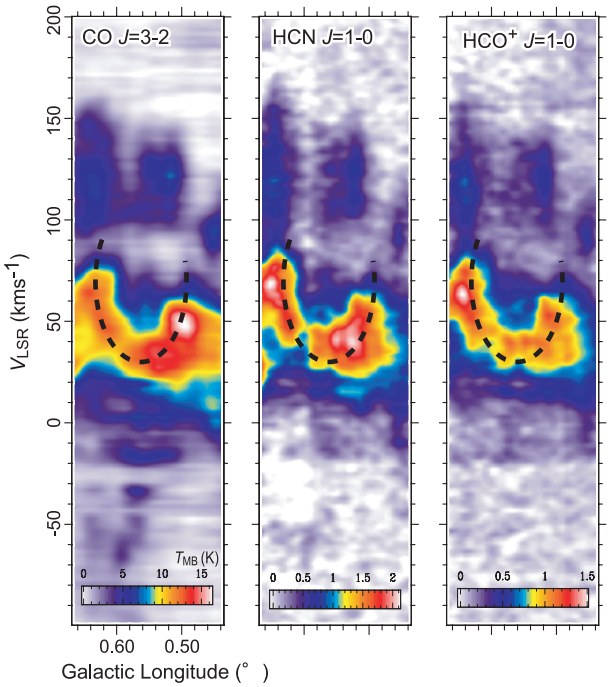

Fig. 2. Longitude–velocity diagrams of the CO $J = 3$–2, HCN $J = 1$–0 and HCO^+ $J = 1$–0 emissions at $b = 0.^\circ07$. The dashed lines represent the model of the expanding motion defined by equation (1).

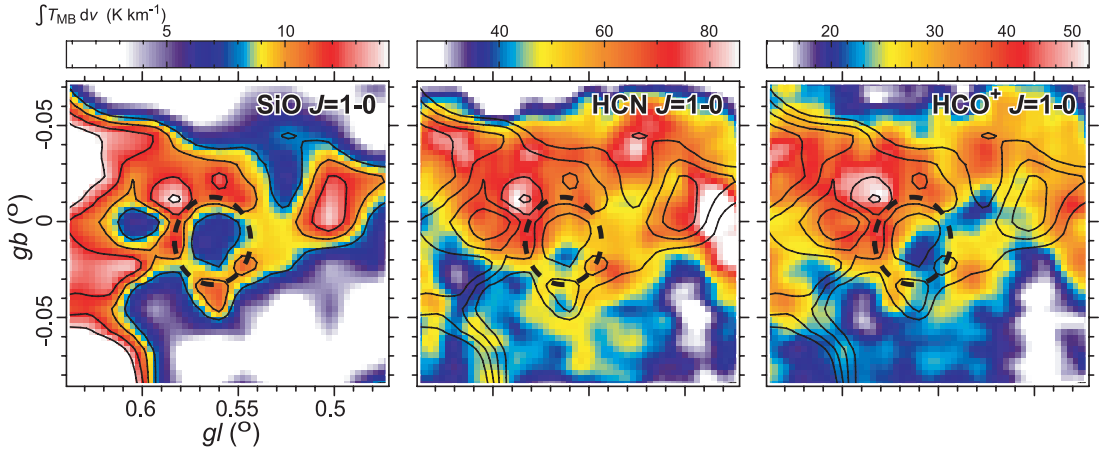

Fig. 3. Integrated intensity maps of the SiO $J = 1$–0, HCN $J = 1$–0 and HCO^+ emissions. The integration range is 35–60 km s^{-1}. The overlaid contours represent the SiO integrated intensity, with levels at 8, 10, 12, and 14 K km s^{-1}. The ellipses are schematic diagrams of the shell with the parameters listed in the table 2.

Table 2. Parameters of the shell/arcs.

	l_0 (°)	b_0 (°)	$r_l \times r_b$ (pc^2)	$v_{\rm LSR}$ (km s^{-1})	$v_{\rm ex}$ (km s^{-1})
CO0.55+0.07	0.571	0.074	8.5 × 6.8	+70	40
SiO0.56−0.01	0.56	−0.01	3.0 × 3.4	—	—

line-of-sight axes,

$$\left(\frac{l-l_0}{r_l}\right)^2+\left(\frac{b-b_0}{r_b}\right)^2+\left(\frac{v-v_0}{v_{\rm exp}}\right)^2=1\,, \qquad (1)$$

where (l_0, b_0) is the center position and v_0 is the systemic velocity, and $r_{l,b}$ are the radii in l and b, respectively. The parameter $v_{\rm exp}$ is the expansion velocity in the line-of-sight direction. Table 2 lists the parameters determined from the CO $J = 3$–2 data by eye-fitting. We assume that the distance to the Galactic Center is 8.5 kpc (Reid et al. 1988). The model of the expanding motion with the parameters in table 2 is presented in figures 1 and 2. Since the velocity channels with $v_{\rm LSR} > 70$ km s^{-1} lack significant emission, $v_{\rm exp}$ could contain a large uncertainty. However, the sizes in the l direction monotonically increase up to $v_{\rm LSR} = 70$ km s^{-1}, which suggests that $v_{\rm exp}$ is at least 40 km s^{-1}.

3.2. *SiO0.56−0.01: SiO Shell*

Figure 3 shows the distribution of the SiO $J = 1$–0 intensity integrated from 30 to 60 km s^{-1}. We found an emission cavity at $(l, b) = (0.^\circ56, -0.^\circ01)$, whose radii are 3.0 pc × 3.4 pc. There are also local minima in the HCN and HCO^+ maps at the position of the SiO cavity. Figure 4 shows l–v maps of CO $J = 3$–2, HCN and HCO^+ at $b = -0.^\circ01$. No clear expanding motion can be traced in the diagrams, but emission lacks in each map within a velocity range of 30–60 km s^{-1}, while the emission at the shell edge has a large velocity width, ∼40 km s^{-1}. The CO $J = 3$–2 emission has a high-velocity wing at the galactic east edge of the SiO shell ($l \sim 0.^\circ57$), which is extended to the ∼20 km s^{-1} velocity channel.

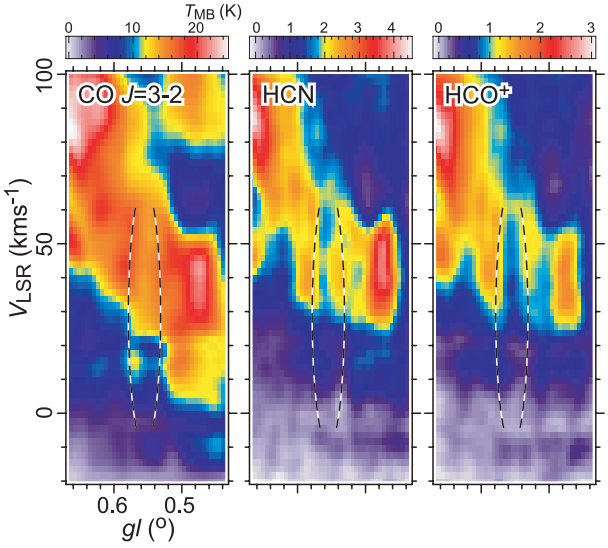

Fig. 4. Longitude–velocity diagrams of the CO $J = 3$–2, HCN $J = 1$–0 and HCO^+ $J = 1$–0 emissions at $b = -0.^\circ01$. The dashed lines represent the edges of the shell SiO0.56−0.01. SiO data is not presented because of its low signal-to-noise ratio, and we present the CO $J = 3$–2 data instead, where a high-velocity wing is observed at the east edge of the shell.

The shell was not found with the CO and ^{13}CO surveys (Oka et al. 1998, 2007), but can be seen in the CS $J = 2$–1 (Tsuboi et al. 1999) and the sub-mm continuum maps (Pierce-Price et al. 2000). The fact that the shell is clearly seen in the SiO data would imply that it consists of shocked molecular gas embedded in less-dense gas, because the SiO molecule is thought to be formed via shock-induced chemistry, and its $J = 1$–0 transition is generally optically thin and has a high critical density of $\sim 10^5$ cm^{-3}.

3.3. *Comparison with Other Wavelengths Data*

We searched for counterparts of the two peculiar molecular features, CO0.55+0.07 and SiO0.56−0.01, at other

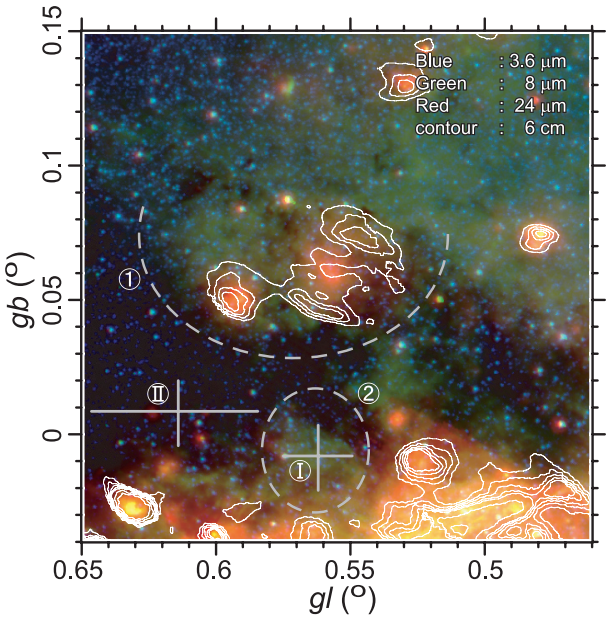

Fig. 5. False color image composed from the IRAC 3.8, 8 μm and the MIPS 24 μm data. The overlaid contour shows the 6-cm continuum distribution taken from the VLA archival data. The cross marks represent the position and the spatial extent of the X-ray sources, G0.61+0.01 and G0.570−0.018, denoted by I and II, respectively. The shapes of CO0.55+0.07 and SiO0.56−0.01 are presented by schematic diagrams, denoted by 1 and 2.

wavelengths. The X-ray astronomical satellite Suzaku took images of the Fe 6.4 and 6.7 keV lines of the Sgr B complex, and identified two diffuse sources (Koyama et al. 2007). Their positions and sizes are displayed in figure 5 by cross marks. On of the X-ray source, G0.570−0.017, is located at the center of the SiO shell. The source was first considered to be a very young SNR with ASUKA and Chandra observations (Senda et al. 2002), but later it is suspected to be an X-ray reflection nebula (XRN), because it has a bright 6.4 keV Fe I line, whose intensity varies with time (Inui et al. 2008). The other source, G0.61+0.01, is bright in the Fe XXVI 6.7 keV line, and thereby is considered to be an SNR. The source overlaps neither of the molecular arc/shells, however.

Figure 5 also presents a contour image of the 6-cm continuum emission taken from the VLA archive image, along with a false-color IR image composed from the IRAC 3.8, 8 μm and the MIPS 24 μm data. There are at least three extended sources in the expanding arc CO0.55+0.07, which are bright in the 6 cm and 24 μm images. They are cataloged as radio continuum sources (OF35A, B, and C), whose ionizing sources were O8.5−9 type stars (Mehringer et al. 1993).

4. Data Analysis

4.1. Mass and Kinetic Energy of CO0.55+0.07

We estimated the mass of the expanding molecular arc CO0.55+0.07. It is difficult to separate the emission that belongs to the arc from the other part, due to the complicated morphology of the molecular clouds. We define the normalized radius from the kinetic center in the l–b–v cube, $R \equiv (\frac{l-l_0}{r_l})^2 + (\frac{b-b_0}{r_b})^2 + (\frac{v-v_0}{v_{\rm exp}})^2$, and take an arbitrary assumption that pixels with $0.8 < R < 1.2$ belong to the arc. The mass is estimated by summing up the hydrogen column densities derived from the ^{13}CO $J = 1$–0 intensity (Oka et al. 1998) by employing the LVG model (Goldreich & Kwan 1974). We assume that $n(\mathrm{H_2})/n(^{13}\mathrm{CO}) = 10^6$ (Lis & Goldsmith 1989, 1990), and that kinetic temperature ($T_{\rm kin}$) and hydrogen density ($n_{\rm H}$) are 28 K and $10^{3.8}$ cm^{-3}, respectively. The temperature and density were derived from the CO $J = 1$–0 and $J = 3$–2 data by an LVG calculation, the details of which are described in the next subsection. The mass was derived to be $10^{5.5}\,M_\odot$. This estimate varies by $\pm 30\%$ when the assumed $T_{\rm kin}$ and $\log_{10} n_{\rm H}$ change by ± 10 K and ± 0.5, respectively.

The above estimate was checked with an independent calculation. We assumed that the gas swept by the arc had a density of $10^{3.8}$ cm^{-3} and a volume filling factor of $\Phi_{\rm A} \lesssim 1$. The mass collected by the expanding arc was calculated by $M = 1.4\, n_{\rm H}\, \mu_{\rm H}\, \Phi_{\rm A}\, V$, where $\mu_{\rm H}$ is the hydrogen mass and $V = \frac{2}{3}\pi (r_l \cdot r_b)^{1.5}$ is the swept volume. The derived mass is $\Phi_{\rm A} 10^{5.6}\,M_\odot$, being consistent with the above estimate.

The kinetic energy of the expanding arc is then estimated to be $\frac{1}{2} M\, {v_{\rm exp}}^2 = 10^{51.5}$ erg or $\Phi_{\rm A} 10^{51.6}$ erg, being comparable to that of the shells in the $l = 1.^\circ 3$ complex (Oka et al. 2001; Tanaka et al. 2007). The kinematic age of the expanding arc is $(r_l\, r_b)^{\frac{1}{2}}\, {v_{\rm exp}}^{-1} = 0.2$ Myr.

The mass of SiO0.56−0.01 is estimated to be $\Phi_{\rm B} 10^{4.3}\,M_\odot$, on the assumption that the shell also consists of swept-up material. The factor $\Phi_{\rm B}$ is the volume filling factor of the preexistent gas. The CO $J = 3$–2 emission at the edges of the shell is extended in the velocity range from 10 km s^{-1} to 60 km s^{-1}, and therefore its expansion velocity should be $\gtrsim 25$ km s^{-1} if it is really expanding. The kinetic energy of the shell is estimated to be $\Phi_{\rm B}\ 10^{50.4}$ erg when $v_{\rm exp} = 25$ km s^{-1}.

4.2. Kinetic Temperature and Density

A correlation plot between the CO $J = 1$–0 and $J = 3$–2 intensities is presented in figure 6. Only the pixels within the range of $0.^\circ 45 < l < 0.^\circ 61$, $-0.^\circ 1 < b < 0.^\circ 1$ and $20\,\mathrm{km\,s^{-1}} < v_{\rm LSR} < 250 \times l\ (^\circ) - 60\,\mathrm{km\,s^{-1}}$ are plotted, in order to exclude the vicinity of the H II regions and the high-velocity region, which are considered to be spatially separated from the main component. There is a tight correlation between the CO $J = 1$–0 and $J = 3$–2 intensities, implying that a large part of the molecular gas has relatively uniform $T_{\rm kin}$ and $n_{\rm H}$.

We estimated typical values of $T_{\rm kin}$ and $n_{\rm H}$ by employing a method of Nagai (2008). We calculated CO $J = 1$–0– CO $J = 3$–2 curves with varying CO column density ($N_{\rm CO}$), and derived the best-fit parameter set of $T_{\rm kin}$ and $n_{\rm H}$ by a least-squares method. The χ^2 value is given by

$$\chi^2 \equiv \sum_i^N {S_i}^2(\mathrm{CO}\,J = 1\text{–}0, \mathrm{CO}\,J = 3\text{–}2)\ , \tag{2}$$

$$ {S_i}^2(X_1, X_2, \ldots) \equiv \sum_{X = X_1, X_2 \ldots} \left[\frac{I_{X,i} - I_{X,\mathrm{LVG}}\,(T_{\rm kin}, n_{\rm H}, N_{\mathrm{CO,i}})}{\sigma_X} \right]^2 , \tag{3}$$

where $N = 3032$ is the number of the pixels, and the degree

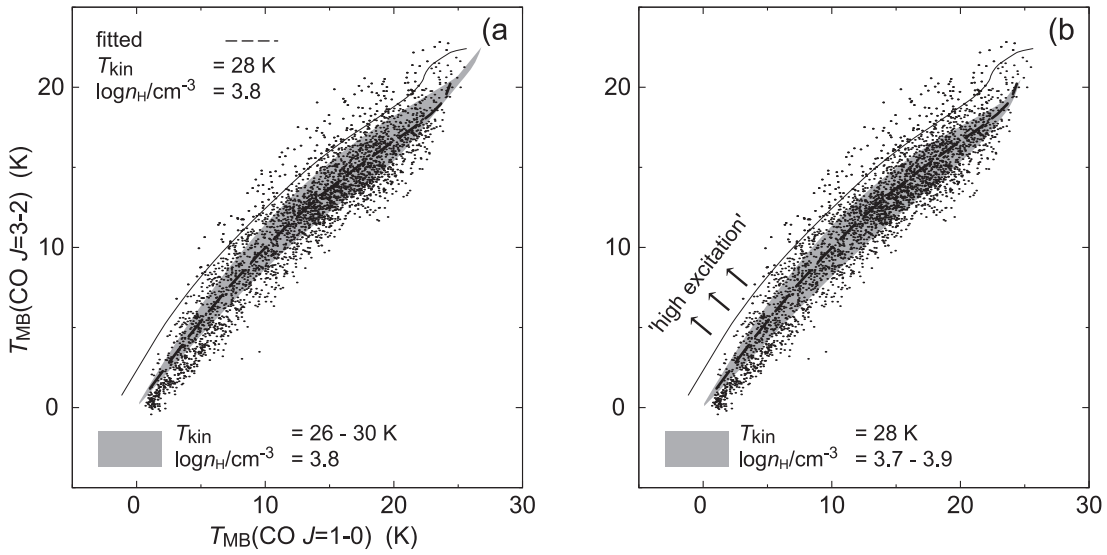

Fig. 6. CO $J = 3$–2 intensity plotted against the CO $J = 1$–0 intensity. The overlaid dashed line is the LVG curve with $T_{\rm kin} = 28$ K and $n_{\rm H} = 10^{3.8}$ cm^{-3}. Curve of S^2(CO $J = 1$–0, CO $J = 3$–2) $= 40$ is also presented with a thin line. The shaded regions in panels (a) and (b) are the area swept by the LVG curves with $T_{\rm kin} = 28 \pm 1$ K and $\log_{10} n_{\rm H} = 3.8 \pm 0.1$, respectively.

of freedom (DOF) is $N - 2$. The values $I_{X,i}$, $I_{X,\rm LVG}$ are the observed and calculated intensities of the transition X, respectively, and σ_X is the rms noise level. The CO column density, $N_{{\rm CO},i}$, is chosen to minimize ${S_i}^2$ at each pixel. The best-fit parameters are $T_{\rm kin} = 28$ K and $n_{\rm H} = 10^{3.8}$ cm^{-3}. The best-fit LVG curve is superposed on figure 6. The filled areas in figures 6a and 6b are the region swept by the LVG curves when the $T_{\rm kin}$ and $\log_{10} n_{\rm H}$ change by ± 2 K and ± 0.1, respectively. The number ratio of the pixels within the area to the total pixels is approximately 60% in each case.

The derived $T_{\rm kin}$ and $n_{\rm H}$ are consistent with the result of Nagai et al. (2007), in which $T_{\rm kin}$ and $n_{\rm H}$ in the 120 pc star forming ring are estimated to be 20–30 K and $10^{3.5-4.0}$ cm^{-3}, respectively. Martin et al. (2004) made an LVG analysis with the CO $J = 1$–0, $J = 4$–3, $J = 7$–6, and ^{13}CO $J = 1$–0 data, and derived a similar density, $n_{\rm H} \sim 10^{3.5-4.0}$ cm^{-3}, but higher temperature, $T_{\rm kin} \sim 40$–50 K. This may be because our analysis is potentially biased toward the lower temperature region, compared to Martin et al. (2004), in which the higher rotational transition lines are used.

4.3. *Detection of High Density Gas*

Several data points are well above the best-fit LVG curve in figure 6, which would represent high-temperature and/or high-density gas. Roughly 10% of the total pixels are above the best-fit curve with the S^2 value being larger than 40, which we arbitrarily define as 'CO $J = 3$–2-enhanced' pixels. We also found pixels with enhanced HCN and HCO$^+$ intensities. In figure 7 the HCN and HCO$^+$ intensities are plotted against the CO $J =$ 1–0 intensity, along with the LVG curves with $T_{\rm kin} = 28$ K and $n_{\rm H} = 10^{3.8}$ cm^{-3}. The LVG curves were calculated by assuming that the [HCN]/[CO] and [HCO$^+$]/[CO] abundance ratios are $10^{-2.7}$ and $10^{-3.9}$, respectively, which were estimated by a least-squares fit, where $T_{\rm kin}$ and $n_{\rm H}$ were fixed. We used only pixels with S^2(CO $J = 1$–0, CO $J = 3$–2) < 1 for the fit. We define the HCN and HCO$^+$ enhanced pixels in a similar manner to the definition of the CO $J = 3$–2-enhancement. The thresholds of the S^2 value are 40 and 25 for the HCN and HCO$^+$ enhancement, respectively.

We classified the pixels with enhanced intensities into three groups, which are considered to trace different physical conditions. The first group (group I) contains pixels where the CO $J = 3$–2 intensity is enhanced, but HCN and HCO$^+$ are not. The second group (group II) is pixels where both of the HCN and HCO$^+$ intensities are enhanced, but CO $J = 3$–2 is not. The pixels where only the HCN or HCO$^+$ intensity is enhanced is excluded in order to reduce the effect of an abundance variation of HCN and HCO$^+$. The third group (group III) is pixels where all of the CO $J = 3$–2, HCN and HCO$^+$ intensities are enhanced.

Figure 8 presents $T_{\rm kin}$ and $n_{\rm H}$ at the pixels of each group, which were calculated with the LVG model without assuming uniformity in $n_{\rm H}$ and $T_{\rm kin}$. A least-squares fit was performed to minimize the local χ^2 value, given by $\chi^2 \equiv S_i$(CO $J = 1$–0, CO $J = 3$–2, HCN, HCO$^+$) at each pixel. The DOF of the fit is 1. Results with a χ^2 larger than 1 were rejected. We also plotted the results for the 'normal' pixels with S(CO $J = 1$–0, CO $J =$ 3–2) < 1. The figure shows that the pixels of groups II and III (colored blue and green in the figure, respectively) represent 'dense gas' with $n_{\rm H} = 10^{4.0-4.5}$ cm^{-3}, while the group I pixels (colored red) represent 'hot gas', having a high $T_{\rm kin}$ of 30–40 K, but $n_{\rm H}$ is similar to that in the normal pixels.

The distribution of the high excitation gas in l–v space is shown in figure 9. There are two main clumps of 'dense gas' with enhanced HCN and HCO$^+$ intensities, both of which are distributed close to the molecular arc and shell; the inner edge of CO0.55+0.07 at $b = 0^\circ.05$, and the galactic-east edge of the SiO0.56−0.01 at $(l, b) = (0^\circ.58, 0^\circ.01)$. This would be evidence that the expanding arc, CO0.55+0.07, consists of shock-compressed material. It could be considered that

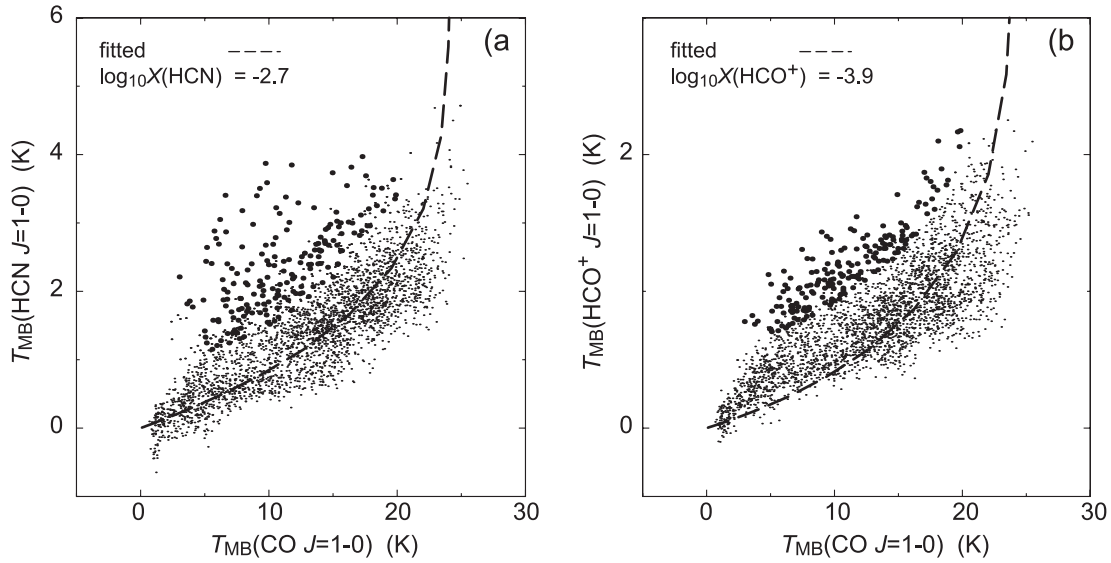

Fig. 7. (a) HCN and (b) HCO^+ intensities plotted against the CO $J = 1$–0 intensity. The best-fit LVG curve with $T_{\rm kin} = 28$ K and $n_{\rm H} = 10^{3.8}$ cm^{-3} is overlaid. Thick marks represent pixels with S^2(CO $J = 1$–0, HCN) > 40 and S^2(CO $J = 1$–0, HCO^+) > 25.

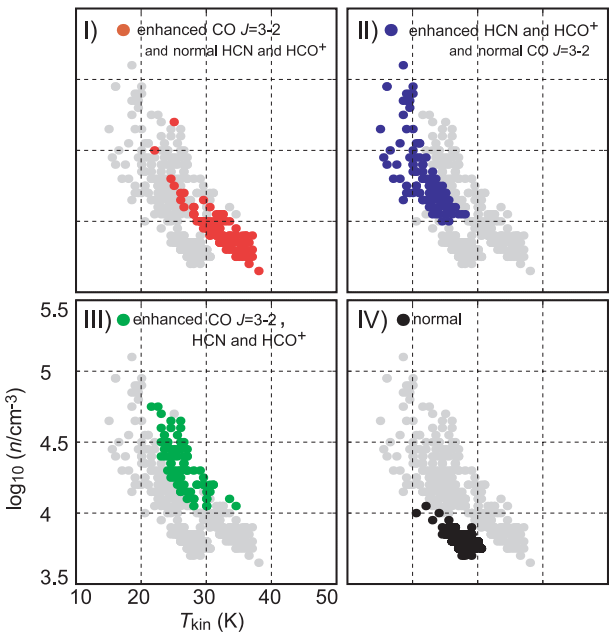

Fig. 8. Density and kinetic temperature in the high excitation region, calculated with the LVG analysis. I) Pixels where only the CO $J =$ 3–2 is enhanced. II) Pixels with enhanced HCN and HCO^+ intensities and normal $J = 3$–2 intensity. III) Pixels where all of the CO $J =$ 3–2, HCN and HCO^+ intensities are enhanced. IV) Normal region.

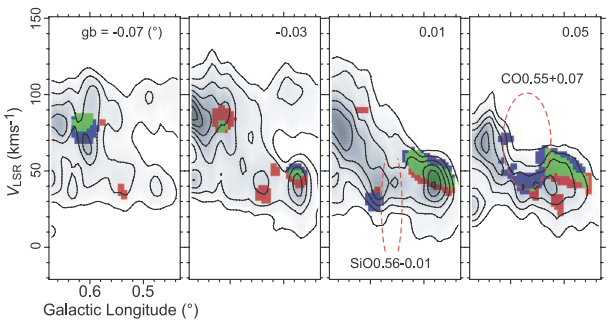

Fig. 9. Distribution of the high excitation region in the l–v diagram. The points are colored in the same manner in the figure 8. The greyscale image represents the HCN intensity.

SiO0.56−0.01 is also a shock-compressed feature, though its expanding motion is not clear in the l–b–v cube. The lack of any enhancement of the CO $J = 3$–2 intensity in these shell/arcs could be understood as that the gathered material has already been cooled via radiation.

There are also high excitation regions that are not associated with the shell/arcs. The two clumps of 'hot gas' at $(l, b) = (0.^\circ60, -0.^\circ03)$ and $(0.^\circ54, -0.^\circ03)$ coincide with the compact H II regions G0.6+0.0-A and Sgr B1-H (Mehringer et al. 1992), respectively, and are likely to be heated by OB stars. There is another large clump of 'dense gas' extended over $(l, b) = (0.^\circ45$–$0.^\circ54, 0.^\circ01$–$0.^\circ05)$, which has enhanced CO $J = 3$–2, HCN and HCO^+ intensities. This region is not associated with any bright radio/IR continuum source, nor to molecular shell/arcs, and hence the excitation mechanism is left as an open question.

4.4. *Abundances of HCN and HCO^+*

The HCN/HCO^+ intensity ratio in the CMZ is known to be higher than that in the galactic disk, ~ 1 (Pratap et al. 1997; Young Owl et al. 2000). The ratio is measured to be ~ 3 in the Circumnuclear Disk and the $l = 1.^\circ3$ complex (Christopher et al. 2005; Tanaka et al. 2007). The ratio in the Sgr B1 complex with our results is ~ 1.5, similar to the galactic disk value. On the other hand, the [HCN]/[CO] abundance ratio was derived to be $\sim 10^{-2.7}$, being more than an order higher than the galactic disk value, $\sim 10^{-4}$ (Pratap et al. 1997; Young Owl et al. 2000), while the $[HCO^+]$/[CO] abundance ratio, $10^{-3.9}$, is similar to the galactic disk value. The high $[HCN]/[HCO^+]$

abundance ratio, $10^{1.2}$, was derived because we assumed a relatively low $n_{\rm H}$, $10^{3.8}\,{\rm cm}^{-3}$. The critical density of the HCN line is nearly an order higher than that of the HCO^+ line, and therefore the HCN/HCO^+ intensity ratio has a positive dependence on $n_{\rm H}$. In order to obtain the best-fit abundance ratio of ~ 1, we assume $n_{\rm H} = 10^6\,{\rm cm}^{-3}$ throughout the complex, which is unlikely, however. Therefore, it would be reasonable to suppose that the $[HCN]/[HCO^+]$ abundance ratio is significantly higher than 1 in the Sgr B1 complex.

5. Discussions

5.1. Origin of the CO Expanding Arc: Supernova Bubble?

The energy source for the expanding arc CO0.55+0.07 should have an energy of $\eta^{-1}\ 10^{51.5}$ erg, where η is the energy conversion efficiency into kinetic energy of the arc. Stellar wind from the O stars in the arc can provide energy of $\sim 10^{49}$ erg within the kinematic age of the arc, and therefore a more energetic source, such as a type-II SN explosion would be required. Given that the energy of a single SN explosion is 10^{51} erg, the required number of SNR is several of η^{-1}.

It is difficult to estimate the precise value of η, but we can assume that η is on order of 0.01–0.1 if the remnant is in the radiative phase. It is plausible that CO0.55+0.07 is radiative, since the cooling time of the SN shell with a density of $10^4\,{\rm cm}^{-3}$ is ~ 100 yr, being much shorter than the kinematic age of the arc, $\tau_{\rm kin} = 2 \times 10^5$ yr. This assumption is also supported by the LVG results presented in figures 8 and 9, where the gas temperature is not higher in the arc than in the other part of the complex. The low η would mean that a single explosion cannot furnish the kinetic energy of the CO arc. Some authors argue that η with multiple explosions could be higher than that with a single explosion, since the adiabatic phase lifetime becomes effectively longer (Melioli & de Gouveia Dal Pino 2004 and references therein).

The CO arc surrounds a group of O8.5−9 stars that accompanies extended 6 cm and 24 μm emission. It could be considered that the stars are 'remnants' of a progenitor cluster of the SN explosions that created the arc. We tested this hypothesis by comparing the numbers of SNe and the O stars, η^{-1} and 3, respectively, with a simple model. We evaluated the χ^2 value given by

$$\chi^2 \equiv \frac{(N_* - 3)^2}{N_*} + \frac{\left(N_{\rm SN} - \eta^{-1}\right)^2}{N_{\rm SN}}\,, \tag{4}$$

where N_* and $N_{\rm SN}$ are the model values of the numbers of O stars and the SN explosions that took place within $\tau_{\rm kin}$, respectively. We made an assumption that the cluster was formed by a short-duration burst, and that the stars in the cluster have the same age. Then, the progenitors of the most recent SNe should have mass similar to those of the most massive members of the current population. We could accordingly assume $N_{\rm SN}/N_* = \delta m_{\rm SN}/\delta m_*$, where $\delta m_* = 1\,M_\odot$ and $\delta m_{\rm SN} = 0.4\,M_\odot$ are the mass ranges of the O stars and the SN progenitors, respectively. The value of $\delta m_{\rm SN}$ was calculated from $\tau_{\rm kin}$ by assuming a mass-age relation with the solar metallicity (Meynet et al. 1994). Then, the DOF of equation (4) is 1 if η is fixed, with N_* being a free parameter. If $\eta > 0.21$ the χ^2 value is < 3.84, which means that the hypothesis cannot be rejected at the 90% confidence level if $\eta > 0.21$.

The cluster mass can be estimated from the most probable value of N_*, when $\eta = 0.21$–0.50, based on the assumption that cluster had a power-low IMF, $dN/dm \propto m^{-\alpha}$. The mass is estimated to be $10^{4.3-4.5}\,M_\odot$ if $\alpha = 2.35$ and the lower/upper cutoffs are $1/100\,M_\odot$. If we assume a flatter IMF with $\alpha = 1.65$ found in the Arches cluster (Figer et al. 1999) and an upper mass cutoff of $20\,M_\odot$, the mass becomes lower, $10^{3.5-3.7}\,M_\odot$, which is still comparable to the mass of the massive clusters in the Galactic Center. This could mean that CO0.55+0.07 is a SN bubble created by a massive cluster that existed in the recent past, similarly to the 'proto-superbubble' in the $l = 1.^\circ3$ complex. CO0.55+0.07 lacks a distinct structure of nonthermal radio emission indicative of SNR, but we note that the SNR candidates found in the X-ray Fe lines are not necessarily associated with known radio SNRs, either. One possible explanation would be that this is due to a high synchrotron loss rate in the strong magnetic field in the CMZ (Oka et al. 2001).

The energy of SiO0.56−0.01, $\Phi_{\rm B} 10^{50.4}$, is by an order smaller than that of CO0.55+0.07, and can be provided by a single SN. The coincidence with the X-ray source G0.570−0.018 may indicate that interaction between the source and the surrounding molecular gas created the SiO shell. The source is considered to be an XRN having a bright feature of the 6.4 keV Fe I Kα emission, but it also contains significant Fe XXV K_α and Fe XX K_α emissions, which are supposed to be emitted by a high-temperature plasma characteristic for SNRs (Inui et al. 2008). These characteristics may imply that SiO0.56−0.01 is a SN bubble at an early stage of the evolution. However, the origin of the X-ray source is still controversial, and further study would be required to confirm the interaction between the source and the surrounding molecular gas.

5.2. Contribution of CO0.55+0.07 to the Turbulent Energy of the CMZ

The expanding arc CO0.55+0.07 is losing its kinetic energy by radiation, while it is collecting mass, and will eventually be mixed with the ambient material when the expansion velocity becomes comparable to the turbulent velocity in the ambient cloud, $\sigma_v = 10\,{\rm km\,s}^{-1}$. As a consequence, a certain fraction of the large kinetic energy of the arc is converted into turbulent energy of the ambient cloud. Based on the assumption that the arc is expanding in the medium with uniform density, both the kinetic energy and the expansion velocity decrease with time as $t^{-3/4}$. Then, the energy input by CO0.55+0.07 is estimated to be $(\sigma_v/v_{\rm exp}) \cdot 10^{51.5}\,{\rm erg} = 10^{50.9}\,{\rm erg}$.

Our question is whether this energy injection has a significant contribution to the energy source for the large velocity width in the CMZ molecular clouds. The dissipation rate of turbulence is estimated to be $1/2\,M_{\rm CMZ}\,{\sigma_v}^3\,l^{-1} = 1 \times 10^{39}\,{\rm erg\,s}^{-1}$ for the entire CMZ, where $M_{\rm CMZ} = 3 \times 10^7\,M_\odot$ is total mass of the CMZ (Dahmen et al. 1998) and $l = 10\,{\rm pc}$ is the scale length of the CMZ clouds (Oka et al. 1998). The rate can also be estimated from the cooling rate of the molecular cloud, which is approximately given by the CO luminosity. The CO luminosity summed over all rotational transitions ($L_{\rm CO}$) can be inferred from the luminosity of the $J = 3$–2 transition (L_{3-2}) by employing an LVG calculation, which shows that $L_{3-2}/L_{\rm CO} = 7.4 \times 10^{-2}$ when $T_{\rm kin} = 40\,{\rm K}$, $n_{\rm H} = 10^4\,{\rm cm}^{-3}$.

We assume that $X_{\rm CO}/\frac{{\rm d}v}{{\rm d}r} = 10^{-4.5}\,{\rm pc\,km\,s^{-1}}$ (Martin et al. 2004) here. We obtained $L_{3-2} = 7.3 \times 10^{37}\,{\rm erg\,s^{-1}}$ from the CO $J = 3$–2 survey data (Oka et al. 2007), which gives that $L_{\rm CO} = 1 \times 10^{39}\,{\rm erg\,s^{-1}}$, in good agreement with the directly calculated value.

The above estimates mean that explosions with the same energy as CO0.55+0.07 are required at a rate of 40–50 ${\rm Myr^{-1}}$ to balance with any turbulent dissipation. Considering the lifetime of CO0.55+0.07, a few 10^5 yr, roughly 10 molecular shell/arcs similar to CO0.55+0.07 should exist in the CMZ if they are main contributors to the turbulent energy. This is not an unrealistic number, since it is known that the CMZ contains a number of molecular shell/arcs and HVCCs, some of which are found to have very large kinetic energy. Recently molecular shells CO1.27+0.01 and CO0.02−0.02 were observed in detail (Tanaka et al. 2007; Oka et al. 2008), and their kinetic energies were estimated to be 10^{51-52} erg. According to Nagai et al. (2008) $\sim$10 HVCCs have kinetic energy larger than 10^{51}. These recent results, including that in this work, may indicate that the local explosive phenomena traced by the molecular shell/arcs and HVCCs have a significant contribution to the turbulent energy in the CMZ.

6. Summary

In this paper we presented the results of a molecular line observation toward the Sgr B1 complex, performed with the NRO 45-m and ASTE 10-m telescopes. The main results and discussions are summarized as below:

1. The expanding molecular arc CO0.55+0.07 is clearly traced by the CO $J = 3$–2, HCN and HCO^+ $J = 1$–0 emissions. The size and the expansion velocity are 8.5 pc $\times$ 6.8 pc and 40 ${\rm km\,s^{-1}}$, respectively.
2. We found an SiO shell extended around the controversial X-ray Fe line source, G0.570−0.018. It is likely that the shell, SiO0.56−0.01, consists of shocked molecular gas embedded in less-dense gas.
3. The kinetic energy of CO0.55+0.07 was derived to be $\Phi_{\rm A}\ 10^{51.5}$ erg. The energy of the SiO shell SiO0.56−0.01 is also estimated to be $\Phi_{\rm B}\ 10^{50.4}$ erg, on the assumption that the shell has expanding motion.
4. Typical kinetic temperature and hydrogen density were derived to be 28 K and $10^{3.8}\,{\rm cm^{-3}}$, respectively, from the CO $J = 1$–0 and $J = 3$–2 intensities. High density clumps with $n_{\rm H} = 10^{4.0-4.5}\,{\rm cm^{-3}}$ were found at the edges of CO0.55+0.07 and SiO0.56−0.01, implying that the arc and the shell consist of swept-up material.
5. The HCN/HCO^+ intensity ratio was measured to be 1.5. The abundance ratio of $[HCN]/[HCO^+]$ is estimated to be very high, $10^{1.2}$, as long as we assume a relatively low density, $10^{3.8}\,{\rm cm^{-3}}$.
6. The kinetic energy of CO0.55+0.07 could be provided by several of η^{-1} SNR explosions within the kinematic age of the arc, 2×10^5 yr. The mass of the progenitor cluster is estimated to be $10^{3.5-4.5}\,M_\odot$, which could mean that CO0.55+0.07 is a SN bubble created by a massive stellar cluster. It is marginally possible that the group of O stars in the arc is a remnant of the SN progenitor cluster.
7. The origin of SiO0.56−0.01 is rather unclear, though it is inferred that the X-ray source G0.570−0.018 is responsible for the shell structure. We suggest that the shell may be an SN bubble at an early stage of evolution, but the origin of the X-ray source is still controversial and further studies would be required.
8. We estimated the energy input by CO0.55+0.07 to the ambient molecular clouds. If there are roughly 10 molecular shell/arcs and HVCCs as energetic as CO0.55+0.07 in the CMZ, they can be significant energy sources for the turbulent energy in the CMZ.

We thank to the referee Dr. Martin for his careful reading and useful comments on our draft paper. We are also grateful to the NRO staffs for their generous support during the observations. Nobeyama Radio Observatory is a branch of the National Astronomical Observatory of Japan, National Institutes of Natural Sciences.

References

Christopher, M. H., Scoville, N. Z., Stolovy, S. R., & Yun, M. S. 2005, ApJ, 622, 346
Dahmen, G., Hüttemeister, S., Wilson, T. L., & Mauersberger, R. 1998, A&A, 331, 959
Figer, D. F., et al. 2002, ApJ, 581, 258
Figer, D. F., Kim, S. S., Morris, M., Serabyn, E., Rich, R. M.,& McLean, I. S. 1999, ApJ, 525, 750
Fukui, Y., et al. 2006, Science, 314, 106
Goldreich, P., & Kwan, J. 1974, ApJ, 190, 27
Hüttemeister, S., Dahmen, G., Mauersberger, R., Henkel, C., Wilson, T. L., & Martín-Pintado, J. 1998, A&A, 334, 646
Inui, T., Koyama, K., Matsumoto, H., & Tsuru, T. G. 2008, astro-ph, 0803.1528v1
Koyama, K., et al. 2007, PASJ, 59, S24
Lee, S., et al. 2008, ApJ, 674, 247
Lis, D. C., & Goldsmith, P. F. 1989, ApJ, 337, 704
Lis, D. C., & Goldsmith, P. F. 1990, ApJ, 356, 195
Martin, C. L., Walsh, W. M., Xiao, K., Lane, A. P., Walker, C. K., & Stark, A. A. 2004, ApJS, 150, 239
Martín-Pintado, J., de Vicente, P., Fuente, A., & Planesas, P. 1997, ApJ, 482, L45
Mehringer, D. M., Yusef-Zadeh, F., Palmer, P., & Goss, W.M. 1992, ApJ, 401, 168
Mehringer, D. M., Palmer, P., Goss, W. M., & Yusef-Zadeh, F. 1993, ApJ, 412, 684
Melioli, C., & de Gouveia Dal Pino, E. M. 2004, A&A, 424, 817
Meynet, G., Maeder, A., Schaller, G., Schaerer, D., & Charbonnel, C. 1994, A&AS, 103, 97
Morris, M., Polish, N., Zuckerman, B., & Kaifu, N. 1983, AJ, 88, 1288
Nagai, M. 2008, Ph.D thesis, The University of Tokyo
Nagai, M., Tanaka, K., Kamegai, K., & Oka, T. 2007, PASJ, 59, 25
Oka, T., Hasegawa, T., Sato, F., Tsuboi, M., & Miyazaki, A. 1998, ApJS, 118, 455

Oka, T., Hasegawa, T., Sato, F., Tsuboi, M., & Miyazaki, A. 2001, PASJ, 53, 797
Oka, T., Hasegawa, T., White, G. J., Sato, F., Tsuboi, M., & Miyazaki, A. 2008 PASJ, 60, 429
Oka, T., Nagai, M., Kamegai, K., Tanaka, K., & Kuboi, N. 2007, PASJ, 59, 15
Paumard, T., et al. 2006, ApJ, 643, 1011
Pierce-Price, D., et al. 2000, ApJ, 545, L121
Pratap, P., Dickens, J. E., Snell, R. L., Miralles, M. P., Bergin, E. A., Irvine, W. M., & Schloerb, F. P. 1997, ApJ, 486, 862
Reid, M. J., Schneps, M. H., Moran, J. M., Gwinn, C. R., Genzel, R., Downes, D., & Rönnäng, B. 1988, ApJ, 330, 809
Requena-Torres, M. A., Martín-Pintado, J., Martín, S., & Morris, M. R. 2008, ApJ, 672, 352
Senda, A., Murakami, H., & Koyama, K. 2002, ApJ, 565, 1017
Tanaka, K., Kamegai, K., Nagai, M., & Oka, T. 2007, PASJ, 59, 323
Tsuboi, M., Handa, T., & Ukita, N. 1999, ApJS, 120, 1
Young Owl, R. C., Meixner, M. M., Wolfire, M., Tielens, A. G. G. M., & Tauber, J. 2000, ApJ, 540, 886